Bai, Long; Kämäräinen, Tero; Xiang, Wenchao; Majoinen, Johanna; Seitsonen, Jani; Grande, Rafael; Huan, Siqi; Liu, Liang; Fan, Yimin; Rojas, Orlando J.

Chirality from Cryo-Electron Tomograms of Nanocrystals Obtained by Lateral Disassembly and Surface Etching of Never-Dried Chitin

Published in:
ACS Nano

DOI:
10.1021/acsnano.0c01327

Published: 23/06/2020

Document Version
Peer-reviewed accepted author manuscript, also known as Final accepted manuscript or Post-print

Please cite the original version:
Bai, L., Kämäräinen, T., Xiang, W., Majoinen, J., Seitsonen, J., Grande, R., Huan, S., Liu, L., Fan, Y., & Rojas, O. J. (2020). Chirality from Cryo-Electron Tomograms of Nanocrystals Obtained by Lateral Disassembly and Surface Etching of Never-Dried Chitin. *ACS Nano*, *14*(6), 6921-6930. https://doi.org/10.1021/acsnano.0c01327

Chirality from cryo-electron tomograms of nanocrystals obtained by lateral disassembly and surface etching of never-dried chitin

Long Bai,[1,4,†,] Tero Kämäräinen,[1,†] Wenchao Xiang,[1,†] Johanna Majoinen,[1] Jani Seitsonen,[2] Siqi Huan,[1,4] Rafael Grande,[1] Liang Liu,[3] Yimin Fan,[3] Orlando J. Rojas[1,3,4*]*

[1] Biobased Colloids and Materials, Department of Bioproducts and Biosystems, Aalto University, P.O. Box 16300, FI-00076 Aalto, Espoo, Finland

[2] Department of Applied Physics, Aalto University, P.O. Box 15100, FI-00076 Aalto, Espoo, Finland

[3] Jiangsu Co-Innovation Center of Efficient Processing and Utilization of Forest Resources, Jiangsu Key Lab of Biomass-Based Green Fuel and Chemicals, College of Chemical Engineering, Nanjing Forestry University, 159 Longpan Road, Nanjing 210037, China

[4] Bioproducts Institute, Departments of Chemical & Biological Engineering, Chemistry, and Wood Science, 2360 East Mall, The University of British Columbia, Vancouver, BC V6T 1Z3, Canada

ABSTRACT

The complex nature of typical colloids and corresponding interparticle interactions pose a challenge in understanding their self-assembly. This specially applies to biological nanoparticles, such as those obtained from chitin, which typically are hierarchical and multidimensional. In this study, we obtain chitin nanocrystals by one-step heterogeneous acid hydrolysis of never-dried crab residues. Partial deacetylation facilitates control over the balance of electrostatic charges (zeta potential in the range between +58 and +75 mV), and therefore

affords chitin nanocrystals (DE-ChNC) with axial aspect (170 to 350 nm in length), as determined by cryogenic TEM and AFM. We find that the surface amines generated by deacetylation, prior to hydrolysis, play a critical role in the formation of individual chitin nanocrystals by the action of a dual mechanism. We directly access the twisting feature of chitin nanocrystals by using electron tomography (ET) and uncover the distinctive morphological differences between chitin nanocrystals extracted from non-deacetylated chitin, ChNC, which are bundled and irregular and DE-ChNC (single, straight nanocrystals). While chitin nanocrystals obtained from dried chitin precursors are known to be twisted and form chiral nematic liquid crystals, our ET measurements indicate no dominant twisting or handedness for the nanocrystals obtained from the never-dried source. Moreover, no separation into typical isotropic and anisotropic phases occur after two months at rest. Altogether, we highlight the critical role of drying the precursors or the nano-polysaccharides to develop chirality.

keywords: Chitin nanocrystals, electron tomography, chirality, surface deacetylation, twist, cryo-TEM

The assembly of nanoscale building blocks into complex supracolloidal architectures potentially leads to easily tailorable functional materials,[1-3] which have shown promise in fields such as controlled delivery,[4] composites,[5,6] photonics,[7] and catalysis.[8] However, any development in these areas requires a deep understanding of interparticle and surface interactions,[9,10] as well as those with the surrounding medium.[11] For example, achieving control on the association and aggregation is imperative to enable constructs with consistent and predictable properties.[12] Biobased nanoparticles and colloids offer special promise given their

chemical and structural characteristics, which are directly encoded within the natural materials they are derived from, be it plants, insects and other sources.[13,14]

Taking advantage of the inherent characteristics of biomass resources, simple top-down strategies have been applied to isolate their building blocks. In this context, cellulose and chitin are examples of some of the most promising biobased colloids.[15-17] Nanocelluloses have been the subject of widespread studies aiming to introduce sustainable functional materials.[18,19] In contrast, the production and utilization of chitin nanoparticles, in particular chitin nanocrystals (ChNC), have remained largely underexplored. Moreover, undertakings that remain pending include the exploitation of the morphological diversity of colloidal chitin as well as its functional attributes.

As a natural polysaccharide,[20] chitin is structured from semicrystalline, tightly-bonded microfibrils that consist of extended linear molecular chains of acetylglucosamine homopolymer, which can develop primary amines at the surface.[21] The microfibril bundles display a fine plywood structure (**Figure 1a**),[22] which is decisive to realize the mechanical strength of chitin-based materials.[23] Similar to cellulose nanocrystals (CNC),[15] spindle-shaped chitin nanocrystals (ChNC) are commonly isolated by strong acid hydrolysis from purified chitin.[24-26] Owing to the positively charged nature that originates from protonated amines on the surface of chitin, ChNC is colloidally stable in aqueous acid medium at a pH $<$ pK_a ($\sim$ 6.3).[27] The amine groups on ChNC structurally originate from respective acetylglucosamine,[28] evolving from the deacetylation of chitin in alkaline condition prior to hydrolysis (**Figure 1a**).[29] Depending on the severity of the process used for ChNC production, it is possible to adjust the

density of amine groups. Importantly, this is in contrast to cellulose nanoparticles, such as cellulose nanofibrils (CNF), which require surface modification of the precursor fibers to install charged groups.[30,31] For instance, given processes and reactive species are demanded for such a purpose, increasing the complexity of the synthesis, its cost and environmental footprint. It is therefore desirable to consider simple and green methods for the production of colloidal chitin and to investigate their properties.

We produced colloidally stable, individualized chitin nanocrystals by surface deacetylation of never-dried chitin followed by acid hydrolysis, termed herein as DE-ChNC. The DE-ChNC was investigated by electron tomography (ET) combined with computational analysis of the 3D reconstructions, and the results were compared with those of non-deacetylated ChNC and chiral nanocellulose.[12,32-34] The ET data provide unique insights into the structure of chitin nanocrystals and their twisting, allowing a better understanding of the role of the naturally-occurring characteristics of chitin and its self-assembly in liquid crystalline phases.

RESULTS AND DISCUSSION

Chitin nanocrystals from never-dried chitin. The procedure used for the isolation of rod-shaped chitin nanocrystals from never-dried and purified α-chitin is shown in **Figure 1a**. First, partially deacetylated chitin (DE-Chitin, 27% amine groups) is obtained by NaOH-induced deacetylation of the purified chitin.[35] The second step, namely, hydrolysis of the obtained DE-Chitin with HCl solution followed by mild ultrasonication, produces positively-charged nanocrystals, DE-ChNC. Herein, the samples are referred to as DE-ChNC30, DE-

ChNC60 and DE-ChNC90, depending on the hydrolysis time (30, 60, and 90 min). In addition, never-dried, purified chitin was directly hydrolyzed for 90 min, e.g., with no intermediate deacetylation in alkaline solution (see schematic illustration in **Figure S4a**), yielding a nanocrystal that is used as a reference, ChNC90. All the DE-ChNCs and ChNC90 are colloidally stable in aqueous suspension and scatter light in the blue region (**Figure S1,** inset). The chemical composition (**Figure S2**) and crystallinity profiles (**Figure S3**) of DE-ChNC90 and ChNC90 are similar,[36] indicating that the deacetylation step, prior to hydrolysis, has no significant influence on such characteristics, which are encoded within the native chitin.

Depending on the preparation route, the morphology of chitin nanocrystals is significantly different in terms of the observed level of particle bundling. *In situ* cryo-TEM imaging of DE-ChNC90 clearly shows individual, well-dispersed rod-like nanocrystals (**Figure 1b**), which are observed in AFM (**Figure 1c** and **1d**). DE-ChNC30 and DE-ChNC60 are also observed as single or individual nanocrystals (cryo-TEM images, **Figure S5**). However, in contrast to the deacetylated nanocrystals (DE-ChNC), bundled crystals are typical in the ChNC90 sample, as shown in the images acquired by cryo-TEM and AFM (**Figure S4b** and **S4c**, respectively). Such feature is more clearly discernible under AFM (**Figure S4c**), especially from line scans across the crystals (inset of **Figure S4c**).

Histograms with Gaussian fit counts (width and length) acquired from TEM imaging of DE-ChNC90 and ChNC90 (along with those corresponding to DE-ChNC30 and DE-ChNC60, **Figure S6**) confirm the measurements from cryo-TEM and AFM (height profiles in **Figure 1d** and **Figure S4c**). Although DE-ChNC90 is slightly shorter and thinner compared with

ChNC90, an identical aspect ratio is determined for both types of nanocrystals (**Table 1**). The nanocrystals obtained at shorter hydrolysis times (DE-ChNC30 and DE-ChNC60) are longer compared with DE-ChNC90 (**Table 1** and **Figure S6**). However, a fairly similar mass yield (~80%) is determined for all the samples (**Table 1**). Likewise, no significant effect of hydrolysis time is observed for the colloidal stability of DE-ChNC in aqueous media (optical transmittance spectra, **Figure S1**). The chemical (FTIR, **Figure S2**) and structural (XRD, **Figure S3**) features of the materials used as precursor are retained in the nanocrystals obtained after short hydrolysis times, presumably given that the surface of DE-Chitin is not fully etched. However, the more remarkable observation relates to the effect of drying: compared to those derived from the never-dried chitin, nanocrystals of similar length obtained from dried chitin powder require significantly more severe hydrolysis conditions (9 h hydrolysis time).[37]

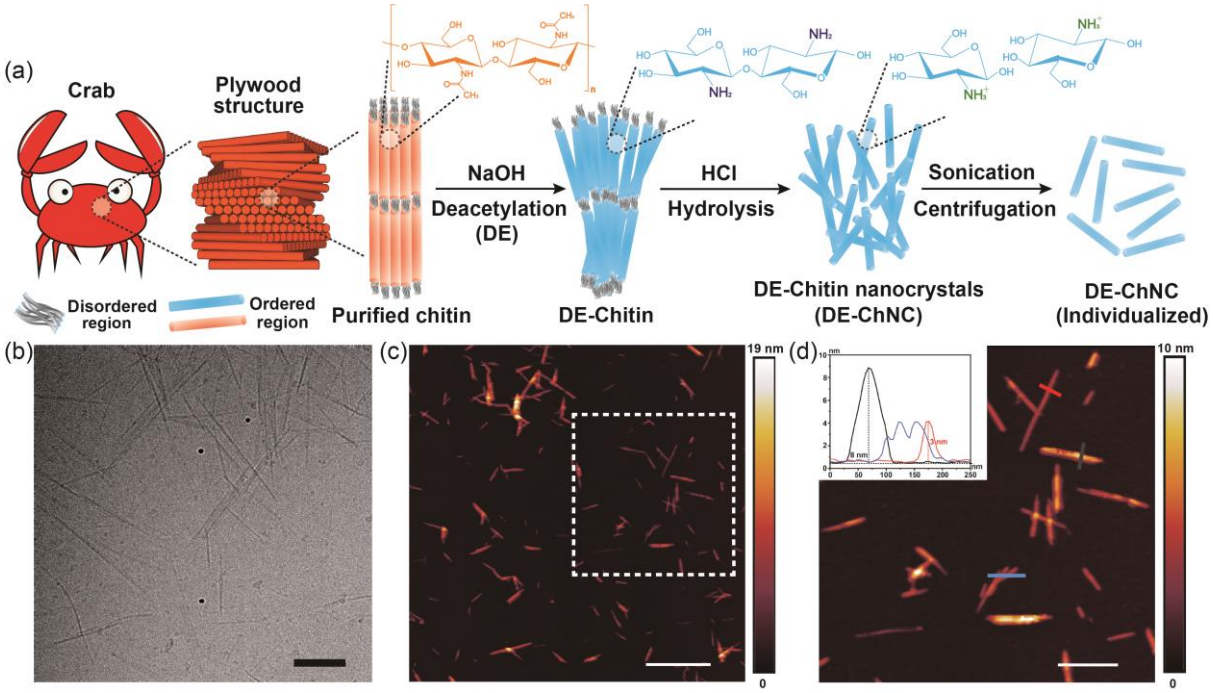

Figure 1. (a) Schematic illustration (not to scale) of the preparation of deacetylated chitin (DE-Chitin) and the corresponding individual chitin nanocrystals (DE-ChNC) by HCl hydrolysis. (b) Cryogenic transmission electron microscope (cryo-TEM) image of DE-ChNC90 (acid

hydrolysis for 90 min). Note: The spherical features in the TEM image correspond to cationic gold nanoparticles that were added for the purpose of alignment (scale bar = 50 nm). (c) Atomic force microscopy (AFM) image of DE-ChNC90 with a rectangle area shown in (d) at higher magnification. The insert in (d) corresponds to the height profiles of three nanocrystals with added scan lines in the cross direction (red, green and blue in the main image). The scale bar in (c) and (d) correspond to 300 and 800 nm, respectively.

Table 1. Main characteristics of chitin nanocrystals (DE-ChNC) obtained after deacetylation followed by hydrolysis with HCl_{aq} for 30, 60 or 90 min.

Sample	DD (%)[2)]	ζ-potential (mV)	Length (nm)[3)]	Width (nm)[3)]	Aspect ratio[3)]	Yield (%)[4)]
DE-ChNC30	10.4 ± 0.6	75 ± 3	357 ± 45	20 ± 4	~18	~83
DE-ChNC60	8.5 ± 0.7	68 ± 2	221 ± 45	13 ± 3	~17	~79
DE-ChNC90	3.3 ± 0.3	60 ± 1	172 ± 29	9 ± 3	~19	~76
ChNC90[1)]	2.2 ± 0.2	58 ± 1	236 ± 47	14 ± 4	~17	~81

[1)] ChNC90 corresponds to a sample that was not deacetylated but directly hydrolyzed for 90 min; [2)] DD = Degree of deacetylation; [3)] The dimension data in this table are extracted from the TEM histograms included in **Figure S5**; [4)] The yield for all the samples was calculated based on the mass of purified, never-dried chitin. The yield of DE-Chitin was approximately 96%.

Deacetylation, surface etching and release of nanocrystals. Deacetylated chitin (DE-Chitin) contains randomly positioned surface amines[35,38] that become charged in acidic condition. The electrostatic charges (ζ-potential, **Table 1**) facilitate nanofibrillation, an effect that is most relevant to disassembly and surface etching (**Figure 2a**), and play important roles in the properties of chitin nanocrystals. These topics are considered in detail in this section.

Since the degree of deacetylation of DE-Chitin is fixed, the DD measured after the given hydrolysis time tracks with the removal or solubilization of the more accessible (surface) deacetylated domains. Thus, as shown in **Table 1**, with the severity of hydrolysis, surface deacetylated chitin is lost, exposing the inner, non-deacetylated fraction. For this reason, DD

is reduced with the extent of hydrolysis (concurrently, the surface charge or zeta potential is reduced). The surface charges are critical in disassembling clusters of hydrolyzed microfibrils, as tested with DE-ChNC30 and DE-ChNC90 prepared in the absence of ultrasonication, which is otherwise applied after dialysis. Indeed, Cryo-TEM images of DE-ChNC30 indicate well fibrillated, individual chitin nanocrystals co-existing with loosely bound chitin nanofibrils (**Figure 2b**, **Figure S7a** and **7b**). The observations, in particular the bundles highlighted in **Figure 2b**, suggest that the binding between microfibrils is weakened by electrostatic repulsion, freeing nanocrystals. As shown in **Figure S7c**, DE-ChNC90 (obtained with no ultrasonication after dialysis) also contains loosely bound, bundled nanocrystals but their lateral dimension is smaller than that of DE-ChNC30. This is likely attributed to the more severe hydrolysis, which facilitates deconstruction of the hydrolyzed nanocrystals.

We further investigate the disassembly of hydrolyzed chitin microfibrils by subjecting DE-Chitin to low-intensity fibrillation. Briefly, DE-Chitin was hydrolyzed and subjected to low-energy ultrasonication after dialysis (during a short time, 30 s). TEM imaging of DE-ChNC60 after such mild treatment indicates incomplete fibrillation of deacetylated chitin microfibrils together with lateral disassembly (**Figure 2c** and **Figure S8a**). DE-ChNC90 shows similar, incomplete disassembly but with smaller bundle dimensions (**Figure S8b**), given the more severe hydrolysis that was applied. Strong ultrasonication readily fibrillates the charged, deacetylated chitin into straight chitin nanofibrils, even in the absence of HCl hydrolysis (**Figure S9**). These results can be rationalized that surface deacetylation of chitin partially prevents intermolecular hydrogen-bonding, breaking the regularity of lateral packing between

chains, which promotes lateral disassembly into nanocrystals after hydrolysis.[29] Taken all together, the observations point to the key role of surface amines on the disassembly of chitin.[35,39]

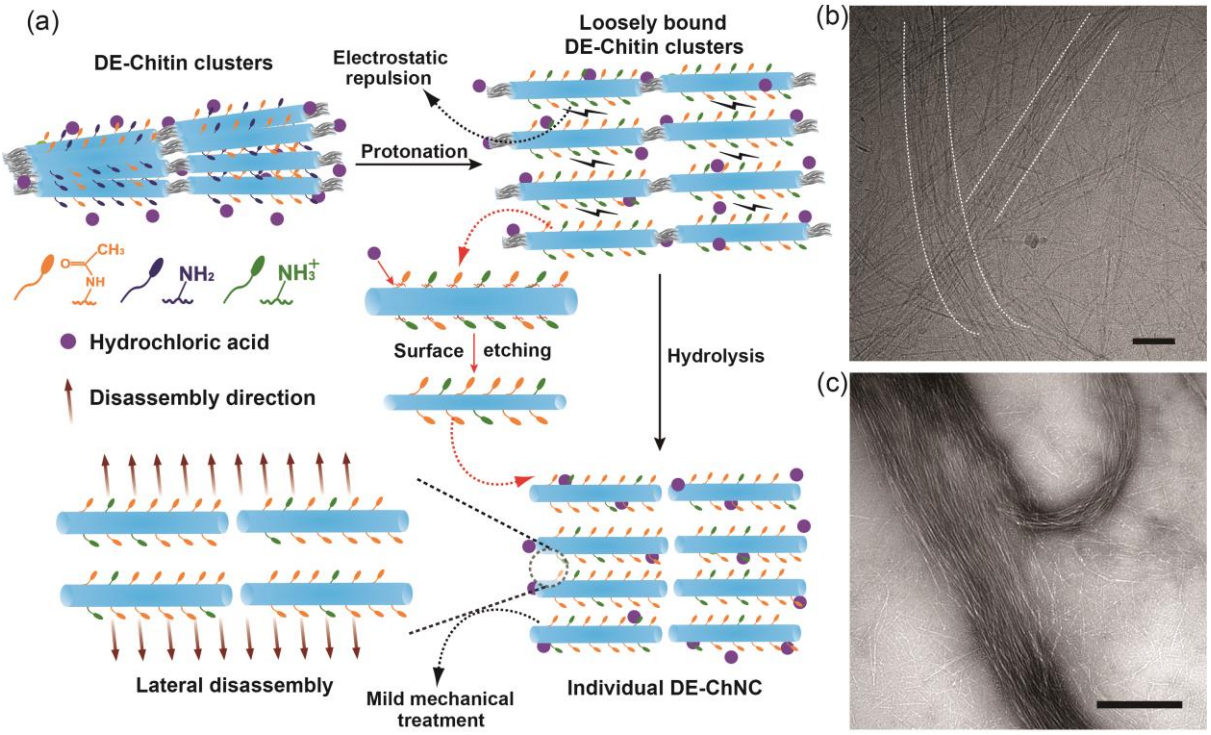

Figure 2. (a) Schematic illustration (not to scale) of the fibrillation of deacetylated chitin clusters that generate single, individual DE-ChNC. (b) Cryo-TEM of DE-ChNC30 in the absence of ultrasonication after dialysis. The spherical features in (b) correspond to reference cationic gold nanoparticles. The dashed lines are added to indicate loosely bound chitin nanofibrils. (c) TEM image of DE-ChNC60 obtained from a suspension that was sonicated after dialysis for 30 s at 30% strength. The scale bars in (b) and (c) correspond to 50 and 500 nm, respectively.

Next, we examine the reason why the degree of deacetylation (DD) of DE-ChNC90 is only slightly higher than that of ChNC90 (extracted from non-deacetylated chitin) (**Table 1** and **Figure S10**), although the initial DD of DE-Chitin was much larger. Indeed, an almost identical ζ-potential is measured for DE-ChNC90 and ChNC90 (**Table 1**). Owing to the insolubility of purified chitin, HCl treatment would mainly result in surface exfoliation (**Figure S4a**),[40] with

little effect on the acetyl groups on chitin's surface, thereby retaining the initially low DD of ChNC90 after hydrolysis (**Table 1**). The more limited etching of the more recalcitrant chitin surfaces leads to a nonhomogeneous reaction. Thus, the more accessible, disordered region is firstly removed upon hydrolysis, generating spindle-like or bundled nanocrystals (**Figure S4**). Since DE-Chitin is relatively more soluble in acidic medium, its surface is readily available for acid etching. As such, lateral and low-ordered regions of chitin are preferentially hydrolyzed and dissolved in acid media.[25]

Inner fibrils in DE-Chitin subjected to hydrolysis are accessible to HCl (**Figure 2a**), given the loosely-bound structure (**Figures 2b**,**2c**). As a result, homogeneous etching is likely to occur, freeing individual nanocrystals of uniform (lateral) size distribution (**Figure 2a**). In fact, the average width of DE-ChNC90 is smaller than that of ChNC90 (**Table 1** and **Figure S6**), which is close to that of individual chitin nanofibrils.[41] Moreover, the aqueous DE-ChNC90 suspension has a higher light transmission (**Figure S1**), indicating smaller nanocrystal size, confirming the enhanced surface etching of deacetylated chitin.

The chitin fibrils located in the inner regions of DE-Chitin are more resistant to acid and etching is limited by the accessibility of HCl. Compared to DE-Chitin, the smaller DD of DE-ChNC90 is the result of surface "etching" of deacetylated chitin upon hydrolysis.[37] On the other hand, DE-ChNC90 retains a slightly higher DD compared to ChNC90 after hydrolysis (**Table 1**), which indicates the effects of different mechanisms. It should be noted that a less severe hydrolysis of DE-Chitin yields a DD value that remains relatively high (**Table 1**), while individual chitin nanocrystals of different dimensions are observed (**Figure S5**), which points

to the fact that surface etching is time-dependent. Taken together, the surface amines generated from deacetylation, prior to hydrolysis, enhance surface etching and play a critical role in the formation of individual chitin nanocrystals, e.g., by the action of a dual mechanism. Deacetylation represents a simple method to expand the property space (morphological and otherwise) of colloidal chitin.

Nanocrystal morphology and bundling. To further examine the main morphological features of DE-ChNC30, DE-ChNC90 and ChNC90, 3D reconstructions from electron tomography (ET) data were obtained from cryo-TEM images (**Figures 3a**,**4a** and **Figures S11-S13**). The mean cross-sectional aspect ratio and length of the nanocrystals were similar for all the reconstructed samples (**Figure S14**), and the reconstructions indicate either single or bundled chitin nanocrystals. As shown in **Figures 3a** and **4a**, individual, straight, rod-like nanocrystals are reconstructed for DE-ChCN90, which directly support our observations related to the morphology of DE-ChNCs. Single nanocrystals dominate the DE-ChNC90 (**Figure S11** and **Table S1**) and DE-ChNC30 (**Figure S13** and **Table S3**) populations. In contrast, although single nanocrystals are observed in the ChNC90 sample (**Figure S12** and **Table S2**), many bundled nanocrystals of relatively irregular shapes are also present (**Figure 4a** and **Figure S12**). Such heterogeneity is in agreement with the uneven etching of non-deacetylated chitin during hydrolysis. In sum, ET reconstructions support the observations from cryo-TEM and AFM but further unveil distinctive morphological differences between DE-ChNC90 (individualized, single, straight nanocrystals) and ChNC90 (single and irregular, bundled nanocrystals).

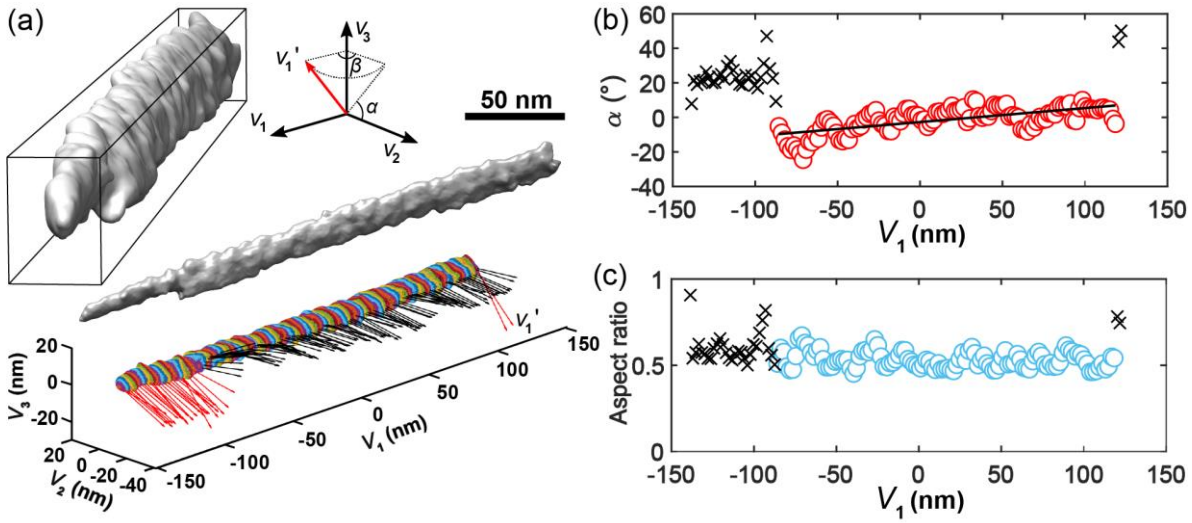

Figure 3. (a) Electron tomography reconstruction of DE-ChNC90 (sample ID: #6, **Table S1**), in two different views, and its representation in the principal component coordinate system (v_1, v_2 and v_3) with cross-sectional segments along v_1 indicated with different colors. Each segment is shown with an arrow (v_1') that denotes its first principal direction, used to determine the segment orientation following angles α and β, as shown by the coordinate system. The α angle is shown in (b) as a function of the segment center coordinate in v_1 with its regression line. The ratio of the segment length along its second and first principal directions, as shown in (c), is used as a local measure of the cross-sectional aspect ratio (thickness/width) of the nanocrystal. The red v_1' and cross markers in (b) denote segments that are excluded from the linear regression model.

Nanocrystals Chirality. We turn our attention to the chiral characteristics of DE-ChNC30, DE-ChNC90 and ChNC90 by using 3D reconstructions with principal component analyses, useful to assess the extent of twisting along the axial direction of the nanocrystals. The morphological chirality concerns the directionality and degree of cross-sectional anisotropy of the nanocrystals, as illustrated in **Figure 3**. To this end, the principal directions of thin segments that are defined perpendicular to the axial direction are analyzed in conjunction with the dimensions of the segments along their second and first principal directions, e.g., to yield

information on the nanocrystal's cross-sectional aspect ratio (thickness/width) (**Figure 3c** and discussion in **Supporting Information**).

Seventeen out of the 28 analyzed DE-ChNC90 nanocrystals showed twisting but with no dominant handedness (8 were right-handed and 9 were left-handed, **Table S1**). Similar observation applies to ChNC90: out of 31 nanocrystals analyzed, 21 were chiral (11 with a left-handed twist and 10 in the opposite direction, **Table S2**). The DE-ChNC30 nanocrystals, obtained at shorter hydrolysis time but with longer average length compared to DE-ChNC90 nanocrystals, display similar particle distribution (chiral *versus* non-chiral): 22 out of 38 are chiral, with a larger portion being left-handed twisted (15 left- and 7 right-handed, **Table S3**). The bundles, when visually apparent, are associated with non-chiral and left/right-handed twists as well as a curved twist profile (**Figure S12**). This is a result of the different non-parallel orientations adopted by the individual nanocrystals (**Figure 4a** and **Table S1-S3**), likely originating from the random nature of the chitin deconstruction. This phenomenon would set the upper limit for the total twist along the crystal length to be 90°, as illustrated in **Figure S15**, which is fulfilled by all chiral nanocrystals in the reconstructions, regardless of whether they are bundled or not (**Table S1-S3**). Thus, the twist magnitude alone cannot be used to decisively distinguish between these two twisting morphologies, as only at larger nanocrystal lengths (over ca. 300 nm) would this difference become more apparent.

No significant differences are observed in the magnitude of the chiral twist among the samples. The average magnitude of the twist angle per unit length of a single nanocrystal, both left- and right-handed, is ca. 0.3 °/nm, while the span of observed twist values increases with

decreasing ChNC length, reaching up to ca. 0.8 °/nm for 50-100 nm nanocrystals (**Figure 4b**). These values are on the lower end of those obtained from molecular dynamic simulation of ~10.6 nm-long α-chitin nanocrystals in aqueous medium (ca. 1-22 °/nm),[42] wherein they observed the largest decrease in chirality as a result of increased number of adjacent chitin chains in the crystal. Herein, the mean cross-sectional aspect ratio does not seem to influence the twist (**Figure 4c**). Comparable twist magnitudes have been observed previously in tomography reconstructions of cellulose nanocrystals (CNC) isolated from Whatman filter paper (~0.2 °/nm),[12] though with a clear twist handedness. A recent electron microdiffraction study of tunicate CNC reports comparably small twist of around 0.04-0.13 °/nm.[43] Similarly, molecular dynamics simulations indicate values ranging between ca. 1-10 °/nm for CNC.[44, 45] Overall, neither chirality nor dominant handedness are observed for never-dried chitin nanocrystals. Therefore, we propose that despite their distinctive morphological features, no difference in chirality exists for DE-ChNC90 and ChNC90 (note that this also applies to the DE-ChNC samples obtained after 30- and 90-min hydrolysis).

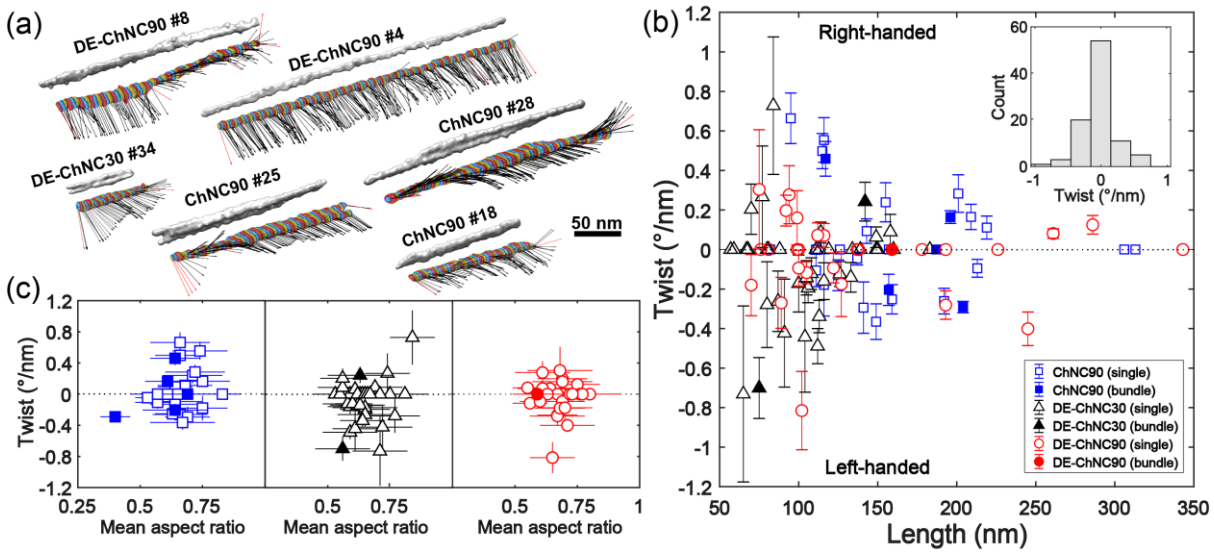

Figure 4. (a) Examples of tomography reconstructions and respective chirality profiles based

on principal component analyses of nanocrystals showing left-handed (single: DE-ChNC90 #8, bundled: DE-ChNC30 #34), right-handed (single: ChNC90 #18, bundled: ChNC90 #25), non-chiral (single: DE-ChNC90 #4) and curved (bundled: ChNC90 #28) twists profiles along their axial direction. Chiral twist (± 99 % confidence interval) of chitin nanocrystals as a function of (b) the axial length and (c) the mean aspect ratio (± standard deviation) of the cross-sectional segments used to determine the twist. Note: Sample reference numbers are included in **Tables S1-S3**.

Our approach presents a direct access to the twisting features of chitin nanocrystals from ET data. Typical chitin nanocrystals are known to form chiral nematic liquid crystals in concentrated suspensions and such assembly is maintained in dried films.[37,46,47] As is the case of CNC, this has been described to be the result of a dominant or unique twisting. In contrast, our ET observations demonstrate no dominant twisting for the types of never-dried chitin nanocrystals considered (at most, the samples were non-chiral). Further evidence is provided from observation of DE-ChNC90 suspended in water (1.2 wt %) for two months, while kept undisturbed, that showed no isotropic/anisotropic phase separation. This relates directly to the optical properties of dry films: DE-ChNC90 suspensions (0.85 wt%) subjected to slow evaporation (drying at ambient temperature) result in transparent film with no cholesteric layering (see film cross-section in **Figure S16**). In summary, no cholesterics of nematic liquid crystals are formed in DE-ChNC90 aqueous suspension nor respective dry film. The ChNC90 suspension (1.2 wt %) does show phase separation but with no spontaneous birefringence, therefore lacking the cholesteric feature of liquid crystalline systems. The lack of chiral nematic phase separation of DE-ChNC and ChNC90 suspensions correlates with the ET observations that indicate no dominant twisting for these never-dried nanocrystals.

Circular dichroism (CD) spectroscopy is a widely used technique to reveal chirality. Unfortunately, no difference in CD signal is observed for cellulose nanocrystals (CNC) at very low concentrations, namely, under conditions that prevent cholesteric liquid crystal formation (tactoids and further phase separation into anisotropic phase) that otherwise hamper detection of twisted individual nanocrystals.[48] The same is expected to apply to chitin nanocrystals. However, it is possible to enhance chirality detection by using plasmonic nanoparticles or chiral molecules attached to the twisted surfaces, leading to supra-structural features that promote, in the case of CNC, enhanced CD detection (CNC right-handed chiral plasmonic features). Such approach can be considered to further validate the conclusions derived from direct ET analyses presented here.

More important to the present discussion is to unveil the origin of the observed differences in chiral properties of dried and never-dried chitin nanocrystals. We hypothesize that the answers relate to the type of (chitin) precursor material: here, never-dried chitin was directly isolated from solid marine biomass residues (exoskeleton of crabs). In contrast, commercially-available, dry-powdered chitin has been used in most studies, and most relevant in a recent related report.[37] This raises the question whether the chirality depends on the history of the sample and its preparation, for instance, comparing once-dried *versus* never-dried materials. Indeed, the effect of water uptake plays an important role in developing cholesteric structures. Dynamic molecular simulation on chitin macromolecules forming fibrils indicates the contribution of twisting,[42] which may be dependent on the hydrogen bonding distribution within the fibrils.[49] However, surrounding water molecules may interact with hydroxyl and

amine groups of chitin, forming hydrogen-bonded networks that counterbalance the natural tendency of chitin chains, thus limiting or preventing twisting of nanocrystals during production. This is in line with our results for chitin nanocrystals from never-dried samples. On the contrary, drying of the precursor chitin can strengthen the hydrogen-bonding network among and within the chains and decrease the specific surface area within the microfibrils,[50] which results in limited accessibility to water (swelling) and chemicals (hydrolysis reagents). Consequently, compared with never-dried samples, chirality may develop in chitin upon drying. Moreover, irreversible bundles may form during drying, which promotes aggregates and coupling of hydrolyzed nanocrystals, facilitating chiral twisting. Taking CNC as a widely studied case, we note that drying CNC after its production enhances its inherent twisting.[43] It is therefore reasonable to assume that similar phenomena apply to chitin nanocrystals upon removal of water, as is likely the case of CNC.[51] Therefore, a standing hypothesis is that the apparent chirality of chitin nanocrystals obtained from once-dried chitin may already exist before their isolation, owing to the formation of extensive hydrogen bonding after removal of water. These effects remain for verification.

Importantly, chirality (or the lack of chirality) of biological nanoparticles is an important consideration for their application. Indeed, twisting and formation of colloidal liquid crystals influence the mechanical performance of related materials. Using the example of CNC, its loading in methyl cellulose/CNC composite fibers cannot be increased without early cholesteric/chiral nematic tactoid formation in the mixed suspension, leading to a limited mechanical performance.[52] Therefore, unidirectionally oriented nanocrystals in a nematic

liquid crystal can be of interest as a precursor to create biobased, defect-free fibers with high mechanical strength.[53]

In sum, as deacetylation generates surface amines in never-dried DE-Chitin, less bundled chitin microfibrils form during HCl treatment, which is the result of electrostatic repulsion and lateral disassembly that stabilize individual nanocrystals. Meanwhile, owing to the already charged chitin surface during DE-ChNC production, it is possible to break the fine balance between electrostatic interactions and torsional elastic energy along the nanocrystal contour length, which partially controls the twisting.[49] This would contribute to a reduction in the chirality of DE-ChNC.

CONCLUSIONS

Individual, rod-like chitin nanocrystals were firstly produced *via* one-step acid-hydrolysis of surface-deacetylated, never-dried chitin. The dimensions of the resultant DE-ChNC depended on the severity of hydrolysis. The mechanism underlying the formation of single nanocrystals involved a synergistic lateral disassembly of chitin fibrils and enhanced surface etching. The introduced deacetylation strategy is expected to expand the versatility of chitin-based colloids, which is naturally encoded in their inherent morphological and chemical features. The 3D morphology of chitin nanoparticles (DE-ChNC) obtained *via* image reconstruction from electron tomography (ET) of cryo-TEM images confirm other complementary experimental evidence. ET reconstructions indicated significant morphological differences between (deacetylated) DE-ChNC and (non-deacetylated, hydrolyzed) ChNC. Chirality evaluation indicate no dominant twisting in both, DE-ChNC90 and ChNC90. We

speculate that the reason underlying such observation is related to the fact that the precursor chitin was never dried.

EXPERIMENTAL SECTION

Purified chitin. α-chitin was purified from fresh crabs (*Callinectes sapidus*) acquired in the local market of Helsinki harbor, Finland. Briefly, crab shells were treated for at least three alternating cycles (1 day each) with 1 M HCl and 1 M NaOH. The residual solid was decolorized by treatment with 0.5 wt% $NaClO_2$ solution (pH 5.0, acetic acid) for 2 h at 70 °C. The purified flake-like chitin was washed with distilled water, and crushed into small pieces with a household blender. The obtained purified, never-dried chitin was stored at 4 °C until further use. NaOH, HCl, $NaClO_2$, and 100 % acetic acid were purchased from Sigma-Aldrich (Helsinki, Finland). Milli-Q water (18.2 MΩ·cm) was purified with a Millipore Synergy UV unit and used throughout the experiments.

Chitin nanocrystals. Firstly, purified chitin was treated with 12.4 M NaOH solution (~33 wt%) at 90 °C for 3.5 h to yield partially deacetylated chitin (DE-Chitin). The liquid-to-solid ratio used in this deacetylation step was equivalent to 25 mL/g. The DE-Chitin was thoroughly washed to reach neutral pH, and excess water was removed at room temperature by pressing. The degree of deacetylation of DE-Chitin was 27.3%, as determined by conductivity titration.[35] Chitin nanocrystals (DE-ChNC) were then produced by HCl hydrolysis of DE-Chitin. Briefly, DE-Chitin was treated under stirring with 3 M HCl (30 mL HCl per solution per g of DE-Chitin) at 95 °C for a time set between 30 and 90 min, depending on the intended severity of the hydrolysis. After the given time, the reaction was quenched by adding a large volume of Milli-

Q water (10-fold), followed by centrifugation at 10000 rpm for 15 min (three times) to remove excess HCl. The bottom volume of the slurry was collected, and dialyzed in Milli-Q water until the pH of the medium reached a value of 4.0. Finally, a titanium tip-sonicator (Sonifier 450, Branson Ultrasonics Co., Danbury, CT, USA) was used with alternating "on" (3 min at a power level set at 30%) and off (5-2 s) cycles. This yield a well dispersed DE-ChNC suspension that was then centrifuged (8000 rpm, 5 min) to remove any remaining large residues, and stored at 4 ℃ before use. The nanochitin samples that were obtained are referred to as DE-ChNC30, DE-ChNC60 and DE-ChNC90, depending on the hydrolysis time.

A nanochitin sample directly hydrolyzed from purified, never-dried chitin was used as a reference. This sample, not subjected to deacetylation, is termed ChNC, which shows at least over 97% degree of acetylation.[37] The procedure for HCl hydrolysis was the same as that for DE-ChNC, and the reaction time was set to 90 min (yielding nanocrystals that are referred to as ChNC90).

Imaging of chitin nanocrystals (ChNC and DE-ChNC). The microstructure of chitin nanocrystals was observed using high-resolution cryogenic transmission electron microscopy (Cryo-TEM, JEM-3200F, JEOL, Japan) operated at 300 kV in bright field mode with Omega-type Zero-loss energy filter. Liquid helium was used in the cryo-TEM. Images were acquired using an Ultrascan 4000 CCD camera (Gatan) with Gatan digital micrograph software. The temperature of the specimen was maintained at -187 ℃ throughout observation. Samples were prepared using FEI Vitrobot Mark IV by placing 3 µL sample suspension (0.005 wt%) on 200 mesh lacey and holey carbon copper grids under 100% humidity, and then blotted with filter

paper. After removing excess liquid, the sample was immediately plunged to -170 ℃ ethane/propane mixture, following cryo-transferring to the microscope. For image alignment, cationic ligand-coated gold nanoparticles (~5 nm) were thoroughly mixed with the sample suspension at a volumetric ratio of 1-to-100 prior to cryogenic preparation.

The morphology of the chitin nanocrystals was also revealed by atomic force microscopy (AFM, Veeco Dimension 5000 scanning probe microscope, Veeco Inc, USA) equipped with NanoScope V controller and HQ:NSC14/Al BS tips (r = 8 nm, MicroMasch, Bulgaria). The tapping mode was used for scanning all samples. Briefly, the respective diluted suspension of chitin nanocrystals (0.001 mg/mL) was dripped onto freshly cleaved mica surface. Excess liquid was removed by blotting from the edge of the mica using filter paper. The samples were dried and stored at room temperature prior to scanning. Modular program (Gwyddion) was used for noise removal and further image analysis.

Electron tomography (ET) of chitin nanocrystals. Due to the vulnerability of chitin nanocrystals to electron beam damage, a tilt series was recorded in a low-dose mode (short record times < 1 s for each tilt angle) with parse tilt angle steps ($> 4°$) using cryo-TEM. This approach did not cause apparent beam damage and allowed high-quality data for ET reconstruction. ET tilt series were acquired using Serial EM software between tilt angles of $+63°$ to $-63°$. Tilt image series was pre-aligned with IMOD and reconstructed using simultaneous iterative reconstruction technique (SIRT) with 8 iterations.[54] A Gaussian smoothing (1.5 nm width) was applied prior to feature extraction of the nanocrystals and their visualization in USCF Chimera software package with a voxel size of ca. 0.56-0.79 nm^3.[55] The

3D reconstructions of chitin nanocrystals were divided into segments along their length direction, which were then analyzed by their principal axis' orientation to characterize the overall nanochitin chirality using an iterative reweighted linear regression model Matlab R2018a (MathWorks) (see details in **Supporting Information**).

ASSOCIATED CONTENT

Supporting Information. Additional information is provided including physicochemical properties of DE-ChNCs and ChNC90 suspensions; cryo-TEM and AFM images of ChNC90; cryo-TEM images for DE-ChNC30 and 60; length and width histograms of DE-ChNCs and ChNC90; cryo-TEM images of DE-ChNC30 and DE-ChNC90 (no ultrasonication treatment); TEM images of DE-ChNC60 and DE-ChNC90 (low-intensity treatment); TEM image of chitin nanofibers; conductometric titration profiles for DE-ChNCs and ChNC90; 3D reconstructions of ChNC90, DE-ChNC30, and DE-ChNC90 nanocrystals; reconstructed dimensions of chitin nanocrystal; schematic model for total twist of bundled ChNC90; SEM images for dried films of DE-ChNC90; and supporting tables for twisting data of chitin nanocrystals and for conductometric titration.

The authors declare no competing financial interest.

AUTHOR INFORMATION

Corresponding Authors

* E-mail: orlando.rojas@ubc.ca Tel: +1-604-822-3457

* E-mail: long.bai@ubc.ca Tel: +1-236-869-0416

Author Contributions

†L.B., T.K. and W.X. contributed equally to this work.

ACKNOWLEDGEMENTS

The authors acknowledge funding from the European Research Council (ERC) under the European Union's Horizon 2020 research and innovation program (ERC Advanced Grant Agreement No. 788489, "BioElCell"), the Canada Excellence Research Chair initiative and the Canada Foundation for Innovation (CFI). R.G. is grateful for the support by the São Paulo Research Foundation (FAPESP, 2017/20891-8). We would like to thank Dr. Nonappa for helpful discussion on the subject of electron tomography.

REFERENCES

(1) Wang, Y.; Wang, Y.; Breed, D. R.; Manoharan, V. N.; Feng, L.; Hollingsworth, A. D.; Weck, M.; Pine, D. J. Colloids with Valence and Specific Directional Bonding. *Nature* **2012**, *491*, 51-55.

(2) Kostiainen, M. A.; Kasyutich, O.; Cornelissen, J. J.; Nolte, R. J. Self-Assembly and Optically Triggered Disassembly of Hierarchical Dendron-Virus Complexes. *Nat. Chem.* **2010**, *2*, 394-399.

(3) Dinsmore, A.; Hsu, M. F.; Nikolaides, M.; Marquez, M.; Bausch, A.; Weitz, D. Colloidosomes: Selectively Permeable Capsules Composed of Colloidal Particles. *Science* **2002**, *298*, 1006-1009.

(4) Chou, L. Y.; Zagorovsky, K.; Chan, W. C. DNA Assembly of Nanoparticle Superstructures for Controlled Biological Delivery and Elimination. *Nat. Nanotechnol.* **2014**, *9*, 148-155.

(5) Zhang, K.; Liimatainen, H. Hierarchical Assembly of Nanocellulose-Based Filaments by Interfacial Complexation. *Small* **2018**, *14*, 1801937.

(6) Huan, S.; Mattos, B. D.; Ajdary, R.; Xiang, W.; Bai, L.; Rojas, O. J. Two-Phase Emulgels for Direct Ink Writing of Skin-Bearing Architectures. *Adv. Funct. Mater.* **2019**, *29*, 1902990.

(7) Hayward, R.; Saville, D.; Aksay, I. A. Electrophoretic Assembly of Colloidal Crystals with Optically Tunable Micropatterns. *Nature* **2000**, *404*, 56-59.

(8) Guo, S.; Sun, S. FePt Nanoparticles Assembled on Graphene as Enhanced Catalyst for Oxygen Reduction Reaction. *J. Am. Chem. Soc.* **2012**, *134*, 2492-2495.

(9) Wang, L.; Xu, L.; Kuang, H.; Xu, C.; Kotov, N. A. Dynamic Nanoparticle Assemblies. *Acc. Chem. Res.* **2012**, *45*, 1916-1926.

(10) Grzelczak, M.; Vermant, J.; Furst, E. M.; Liz-Marzan, L. M. Directed Self-Assembly of Nanoparticles. *ACS Nano* **2010**, *4*, 3591-3605.

(11) Min, Y.; Akbulut, M.; Kristiansen, K.; Golan, Y.; Israelachvili, J. The Role of Interparticle and External Forces in Nanoparticle Assembly. In *Nanoscience and Technology: A Collection of Reviews from Nature Journals*, World Scientific: Singapore, 2009.
(12) Majoinen, J.; Haataja, J. S.; Appelhans, D.; Lederer, A.; Olszewska, A.; Seitsonen, J.; Aseyev, V.; Kontturi, E.; Rosilo, H.; Österberg, M. Supracolloidal Multivalent Interactions and Wrapping of Dendronized Glycopolymers on Native Cellulose Nanocrystals. *J. Am. Chem. Soc.* **2014**, *136*, 866-869.
(13) Ozin, G. A.; Arsenault, A.; Cademartiri, L. *Nanochemistry: A Chemical Approach to Nanomaterials: Edition 2*, Royal Society of Chemistry: London, 2015.
(14) Bai, L.; Greca, L. G.; Xiang, W.; Lehtonen, J.; Huan, S.; Nugroho, R. W. N.; Tardy, B. L.; Rojas, O. J. Adsorption and Assembly of Cellulosic and Lignin Colloids at Oil/water Interfaces. *Langmuir* **2018**, *35*, 571-588.
(15) Habibi, Y.; Lucia, L. A.; Rojas, O. J. Cellulose Nanocrystals: Chemistry, Self-assembly, and Applications. *Chem. Rev.* **2010**, *110*, 3479-3500.
(16) Duan, B.; Huang, Y.; Lu, A.; Zhang, L. Recent Advances in Chitin Based Materials Constructed *via* Physical Methods. *Prog. Polym. Sci.* **2018**, *82*, 1-33.
(17) Zhu, Y.; Romain, C.; Williams, C. K. Sustainable Polymers from Renewable Resources. *Nature* **2016**, *540*, 354-362.
(18) Kontturi, E.; Laaksonen, P.; Linder, M. B.; Gröschel, A. H.; Rojas, O. J.; Ikkala, O. Advanced Materials through Assembly of Nanocelluloses. *Adv. Mater.* **2018**, *30*, 1703779.
(19) Wang, X.; Yao, C.; Wang, F.; Li, Z. Cellulose-Based Nanomaterials for Energy Applications. *Small* **2017**, *13*, 1702240.
(20) Ling, S.; Chen, W.; Fan, Y.; Zheng, K.; Jin, K.; Yu, H.; Buehler, M. J.; Kaplan, D. L. Biopolymer Nanofibrils: Structure, Modeling, Preparation, and Applications. *Prog. Polym. Sci.* **2018**, *85*, 1-56.
(21) Rinaudo, M. Chitin and Chitosan: Properties and Applications. *Prog. Polym. Sci.* **2006**, *31*, 603-632.
(22) Oh, D. X.; Cha, Y. J.; Nguyen, H.-L.; Je, H. H.; Jho, Y. S.; Hwang, D. S.; Yoon, D. K. Chiral Nematic Self-Assembly of Minimally Surface Damaged Chitin Nanofibrils and Its Load Bearing Functions. *Sci. Rep.* **2016**, *6*, 23245.
(23) Suksangpanya, N.; Yaraghi, N. A.; Kisailus, D.; Zavattieri, P. Twisting Cracks in Bouligand Structures. *J. Mech. Behav. Biomed. Mater.* **2017**, *76*, 38-57.
(24) Goodrich, J. D.; Winter, W. T. α-Chitin Nanocrystals Prepared from Shrimp Shells and Their Specific Surface Area Measurement. *Biomacromolecules* **2007**, *8*, 252-257.
(25) Zeng, J.-B.; He, Y.-S.; Li, S.-L.; Wang, Y.-Z. Chitin Whiskers: An Overview. *Biomacromolecules* **2011**, *13*, 1-11.
(26) Gopalan Nair, K.; Dufresne, A. Crab Shell Chitin Whisker Reinforced Natural Rubber Nanocomposites. 1. Processing and Swelling Behavior. *Biomacromolecules* **2003**, *4*, 657-665.
(27) Li, J.; Revol, J.; Marchessault, R. Rheological Properties of Aqueous Suspensions of Chitin Crystallites. *J. Colloid Interface Sci.* **1996**, *183*, 365-373.
(28) Fan, Y.; Saito, T.; Isogai, A. Individual Chitin Nano-Whiskers Prepared from Partially Deacetylated α-Chitin by Fibril Surface Cationization. *Carbohydr. Polym.* **2010**, *79*, 1046-

1051.
(29) Li, J.; Revol, J. F.; Marchessault, R. Effect of Degree of Deacetylation of Chitin on the Properties of Chitin Crystallites. *J. Appl. Polym. Sci.* **1997**, *65*, 373-380.
(30) Saito, T.; Kimura, S.; Nishiyama, Y.; Isogai, A. Cellulose Nanofibers Prepared by TEMPO-Mediated Oxidation of Native Cellulose. *Biomacromolecules* **2007**, *8*, 2485-2491.
(31) Ishii, D.; Saito, T.; Isogai, A. Viscoelastic Evaluation of Average Length of Cellulose Nanofibers Prepared by TEMPO-Mediated Oxidation. *Biomacromolecules* **2011**, *12*, 548-550.
(32) Ciesielski, P. N.; Matthews, J. F.; Tucker, M. P.; Beckham, G. T.; Crowley, M. F.; Himmel, M. E.; Donohoe, B. S. 3D Electron Tomography of Pretreated Biomass Informs Atomic Modeling of Cellulose Microfibrils. *ACS Nano* **2013**, *7*, 8011-8019.
(33) Usov, I.; Nyström, G.; Adamcik, J.; Handschin, S.; Schütz, C.; Fall, A.; Bergström, L.; Mezzenga, R. Understanding Nanocellulose Chirality and Structure-Properties Relationship at the Single Fibril Level. *Nat. Commun.* **2015**, *6*, 7564.
(34) Nyström, G.; Arcari, M.; Adamcik, J.; Usov, I.; Mezzenga, R. Nanocellulose Fragmentation Mechanisms and Inversion of Chirality from the Single Particle to the Cholesteric Phase. *ACS Nano* **2018**, *12*, 5141-5148.
(35) Bai, L.; Huan, S.; Xiang, W.; Liu, L.; Yang, Y.; Nugroho, R. W. N.; Fan, Y.; Rojas, O. J. Self-Assembled Networks of Short and Long Chitin Nanoparticles for Oil/water Interfacial Superstabilization. *ACS Sustainable Chem. Eng.* **2019**, *7*, 6497-6511.
(36) Ding, B.; Cai, J.; Huang, J.; Zhang, L.; Chen, Y.; Shi, X.; Du, Y.; Kuga, S. Facile Preparation of Robust and Biocompatible Chitin Aerogels. *J. Mater. Chem.* **2012**, *22*, 5801-5809.
(37) Narkevicius, A.; Steiner, L. M.; Parker, R. M.; Ogawa, Y.; Frka-Petesic, B.; Vignolini, S. Controlling the Self-Assembly Behavior of Aqueous Chitin Nanocrystal Suspensions. *Biomacromolecules* **2019**, *20*, 2830-2838.
(38) Liu, L.; Bai, L.; Tripathi, A.; Yu, J.; Wang, Z.; Borghei, M.; Fan, Y.; Rojas, O. J. High Axial Ratio Nanochitins for Ultrastrong and Shape-Recoverable Hydrogels and Cryogels *via* Ice Templating. *ACS Nano* **2019**, *13*, 2927-2935.
(39) Liu, L.; Borghei, M.; Wang, Z.; Xu, J.; Fan, Y.; Rojas, O. J. Salt-Induced Colloidal Destabilization, Separation, Drying, and Redispersion in Aqueous Phase of Cationic and Anionic Nanochitins. *J. Agric. Food Chem.* **2018**, *66*, 9189-9198.
(40) Chen, Y.; Liu, Z.; Li, M.; Wu, X.; You, J.; Li, C. Guiding Growth Orientation of Two-Dimensional Au Nanocrystals with Marine Chitin Nanofibrils for Ultrasensitive and Ultrafast Sensing Hybrids. *J. Mater. Chem. B* **2017**, *5*, 9502-9506.
(41) Al-Sawalmih, A.; Li, C.; Siegel, S.; Fabritius, H.; Yi, S.; Raabe, D.; Fratzl, P.; Paris, O. Microtexture and Chitin/calcite Orientation Relationship in the Mineralized Exoskeleton of the American Lobster. *Adv. Funct. Mater.* **2008**, *18*, 3307-3314.
(42) Střelcová, Z.; Kulhánek, P.; Friák, M.; Fabritius, H.-O.; Petrov, M.; Neugebauer, J.; Koča, J. The Structure and Dynamics of Chitin Nanofibrils in An Aqueous Environment Revealed by Molecular Dynamics Simulations. *RSC Adv.* **2016**, *6*, 30710-30721.
(43) Ogawa, Y. Electron Microdiffraction Reveals the Nanoscale Twist Geometry of Cellulose Nanocrystals. *Nanoscale* **2019**, *11*, 21767-21774.

(44) Matthews, J. F.; Skopec, C. E.; Mason, P. E.; Zuccato, P.; Torget, R. W.; Sugiyama, J.; Himmel, M. E.; Brady, J. W. Computer Simulation Studies of Microcrystalline Cellulose Iβ. *Carbohydr. Res.* **2006**, *341*, 138-152.

(45) Zhao, Z.; Shklyaev, O. E.; Nili, A.; Mohamed, M. N. A.; Kubicki, J. D.; Crespi, V. H.; Zhong, L. Cellulose Microfibril Twist, Mechanics, and Implication for Cellulose Biosynthesis. *J. Phys. Chem. A* **2013**, *117*, 2580-2589.

(46) Li, J.; Revol, J.; Naranjo, E.; Marchessault, R. Effect of Electrostatic Interaction on Phase Separation Behaviour of Chitin Crystallite Suspensions. *Int. J. Biol. Macromol.* **1996**, *18*, 177-187.

(47) Tzoumaki, M. V.; Moschakis, T.; Biliaderis, C. G. Metastability of Nematic Gels Made of Aqueous Chitin Nanocrystal Dispersions. *Biomacromolecules* **2009**, *11*, 175-181.

(48) Majoinen, J.; Hassinen, J.; Haataja, J. S.; Rekola, H. T.; Kontturi, E.; Kostiainen, M. A.; Ras, R. H.; Törmä, P.; Ikkala, O. Chiral Plasmonics Using Twisting Along Cellulose Nanocrystals as A Template for Gold Nanoparticles. *Adv. Mater.* **2016**, *28*, 5262-5267.

(49) Adamcik, J.; Mezzenga, R. Adjustable Twisting Periodic Pitch of Amyloid Fibrils. *Soft Matter* **2011**, *7*, 5437-5443.

(50) Agarwal, U. P.; Ralph, S. A.; Reiner, R. S.; Baez, C. Probing Crystallinity of Never-Dried Wood Cellulose with Raman Spectroscopy. *Cellulose* **2016**, *23*, 125-144.

(51) Beck, S.; Bouchard, J.; Berry, R. Dispersibility in Water of Dried Nanocrystalline Cellulose. *Biomacromolecules* **2012**, *13*, 1486-1494.

(52) Hynninen, V.; Mohammadi, P.; Wagermaier, W.; Hietala, S.; Linder, M. B.; Ikkala, O. Methyl Cellulose/Cellulose Nanocrystal Nanocomposite Fibers with High Ductility. *Eur. Polym. J.* **2019**, *112*, 334-345.

(53) Mittal, N.; Ansari, F.; Gowda. V, K.; Brouzet, C.; Chen, P.; Larsson, P. T.; Roth, S. V.; Lundell, F.; Wagberg, L.; Kotov, N. A. Multiscale Control of Nanocellulose Assembly: Transferring Remarkable Nanoscale Fibril Mechanics to Macroscale Fibers. *ACS Nano* **2018**, *12*, 6378-6388.

(54) Kremer, J. R.; Mastronarde, D. N.; McIntosh, J. R. Computer Visualization of Three-Dimensional Image Data Using IMOD. *J. Struct. Biol.* **1996**, *116*, 71-76.

(55) Pettersen, E. F.; Goddard, T. D.; Huang, C. C.; Couch, G. S.; Greenblatt, D. M.; Meng, E. C.; Ferrin, T. E. UCSF Chimera-A Visualization System for Exploratory Research and Analysis. *J. Comput. Chem.* **2004**, *25*, 1605-1612.